This paper is available on line at http://www.mcponline.org

# HSV-1 CgaI$^+$ Infection Promotes Quaking RNA Binding Protein Production and Induces Nuclear-Cytoplasmic Shuttling of Quaking I-5 Isoform in Human Hepatoma Cells*[S]

**Virginia Sánchez-Quiles‡, María I. Mora‡, Victor Segura‡, Anna Greco§, Alberto L. Epstein§, Maria Giovanna Foschini¶, Loïc Dayon‖, Jean-Charles Sanchez‖, Jesús Prieto‡, Fernando J. Corrales‡¶, and Enrique Santamaría‡**¶**

**Herpesvirus type 1 (HSV-1) based oncolytic vectors arise as a promising therapeutic alternative for neoplastic diseases including hepatocellular carcinoma. However, the mechanisms mediating the host cell response to such treatments are not completely known. It is well established that HSV-1 infection induces functional and structural alterations in the nucleus of the host cell. In the present work, we have used gel-based and shotgun proteomic strategies to elucidate the signaling pathways impaired in the nucleus of human hepatoma cells (Huh7) upon HSV-1 CgaI$^+$ infection. Both approaches allowed the identification of differential proteins suggesting impairment of cell functions involved in many aspects of host-virus interaction such as transcription regulation, mRNA processing, and mRNA splicing. Based on our proteomic data and additional functional studies, cellular protein quaking content (QKI) increases 4 hours postinfection (hpi), when viral immediate-early genes such as ICP4 and ICP27 could be also detected. Depletion of QKI expression by small interfering RNA results in reduction of viral immediate-early protein levels, subsequent decrease in early and late viral protein content, and a reduction in the viral yield indicating that QKI directly interferes with viral replication. In particular, HSV-1 CgaI$^+$ induces a transient increase in quaking I-5 isoform (QKI-5) levels, in parallel with an enhancement of p27$^{Kip1}$ protein content. Moreover, immunofluorescence microscopy showed an early nuclear redistribution of QKI-5, shuttling from the nucleus to the cytosol and colocalizing with nectin-1 in cell to cell contact regions at 16–24 hpi. This evidence sheds new light on mechanisms mediating hepatoma cell response to HSV-1 vectors highlighting QKI as a central molecular mediator.** ***Molecular & Cellular Proteomics 10: 10.1074/mcp.M111.009126, 1–14, 2011.***

Herpesvirus type 1 (HSV-1)[1] is a large, double-stranded DNA virus with a genome of 153 kbp, encoding at least 89 proteins. HSV-1 replicates in the nucleus of the host cell and its gene expression follows a temporal pattern including three stages: immediate early (IE), early (E), and late (L) genes (1). The HSV genome is replicated via a rolling circle mechanism. It commences around 3–4 hours postinfection (hpi) reaching maximum efficiency between 8–16 hpi (2), taking a single round of lytic replication from viral entry to release ~16–20 h in permissive tissue culture cells (3). The process of infection begins when the virions bind heparan sulfate moieties present on host cell surfaces. Within the first 30 min of infection, the initial attachment triggers a cascade of molecular interactions involving multiple viral and host cell proteins and receptors, leading to penetration of the viral nucleocapsid and tegument proteins into the cytoplasm (4). After penetration, viral capsids and associated tegument proteins interact with dynein and use the microtubule network to transit the cytosol to the nuclear envelope, where they dock with nuclear pores and release their uncoated genomes in the nucleoplasm for viral transcription and replication. The temporal program of viral gene expression is highly regulated (5, 6). The first genes transcribed during viral infection are the IE genes that serve as transactivators of E genes. E proteins include the enzymes

From the ‡Division of Hepatology and Gene Therapy, Proteomics and Bioinformatics Unit, Centre for Applied Medical Research (CIMA), University of Navarra, 31008 Pamplona, Spain, §Université de Lyon, UCB-Lyon 1, Lyon, F-69003, France; CNRS, UMR5534, Centre de Génétique Moléculaire et Cellulaire, 16 rue Dubois, Villeurbanne, F-69622, France, ¶Department of Experimental and Diagnostic Medicine - Section of Microbiology, University of Ferrara, Via Luigi Borsari 46, 44100 Ferrara, Italy, ‖Department of Structural Biology and Bioinformatics, Biomedical Proteomics Group, Geneva University, Geneva 4, Geneva 1211, Switzerland

Received February 28, 2011

Published, MCP Papers in Press, April 5, 2011, DOI 10.1074/mcp.M111.009126

[1] The abbreviations used are: HSV-1, Herpes Simplex Virus Type-1; HCC, Hepatocellular carcinoma; MOI, multiplicity of infection; pfu, plaque forming units; hpi, hours post infection; IEF, isoelectric focusing; QKI, Protein quaking; LC, Liquid chromatography; ESI, Electrospray ionization; MS/MS, Tandem mass spectrometry; two-dimensional-DIGE, two-dimensional difference gel electrophoresis; TMT, Tandem mass tag; LTQ, Linear ion trap.

that are required for replication of the viral genome. The temporal program of HSV-1 gene expression ends with the appearance of the L genes, which constitute the structural proteins of the virus. Functional IE proteins are required for the synthesis of all the virally encoded proteins (7). At the same time, the virus acts to inhibit host cell RNA metabolism via a mechanism called virion host shutoff (8), causing a destabilization of mRNAs and cellular polyribosomes (9). The virion host shutoff is supplemented soon after infection by a concomitant inhibition of host cellular protein synthesis and RNA splicing mediated by the immediate-early HSV-1 ICP27 protein (10). These alter cellular transcription and RNA processing factors such as polyadenylation factors and the phosphorylation state of RNA polymerase II (11) to transcribe the viral genome at the expense of its host cell. Although the synthesis of most cellular proteins is progressively inhibited during the course of infection, some specific cellular proteins continue to be efficiently synthesized, even during the late phase (12, 13). Recent studies have used different protein separation methods and relative quantification strategies to study the cellular response to different viral infections (14). Comparative proteomics based on a combination of 2-DE with mass spectrometry (MS) has been used to describe protein profiles of HSV-1-infected cells (3, 15, 16). In targeted-proteomic studies, it has been described that HSV-1 VP19C and VP26 proteins associate to ribosomes in HeLa cells (13), and HSV-1 ICP8 and ICP27 interact directly with members of large cellular complexes involved in cellular translation, replication, and chromatin remodelling suggesting new insights into viral replication mechanisms (17, 18).

Hepatocellular carcinoma (HCC) is one of the most common malignancies worldwide with a global annual incidence of nearly 1 million cases (19) and an estimated 600,000 deaths per year (20). Although the identification of the main risk factors and the routine screening of the population at risk may lead to the early diagnosis of HCC, the prognosis is poor mainly because of the aggressiveness of the lesions at the time of diagnosis and also to the lack of effective therapies. The development of HSV-1-based oncolytic vectors (21) strengthened by induction of oncoapoptosis (22, 23), is a promising research approach to target specifically and efficiently human cancer cells (23, 24). Because cancer cells are especially sensitive to apoptosis induced by modified HSV-1 strains (23, 25, 26), there is an increasing interest in the identification of cellular intermediates orchestrating the host tumoral cell response to HSV-1 strains to promote the development of more efficient and specific vectors. By comparative cytosolic and microsomal proteome analysis we have previously identified erlin-2, Bif-1, RuvB-like 2, and PP2A as novel HSV-1 Cgal$^+$ targets involved in the regulation of human hepatoma cell death. The deregulation of the Raf/MAP kinase and FAK/PI3K/Akt survival routes together with the impairment of the mitochondrial apoptotic pathway involving the activation and deactivation of Bcl2 family members and the activation of caspase 3 late in infection (24 hpi) were, at least in part, the effector processes responsible for Huh7 cell death (16). To gain insight on the mechanisms orchestrating the Huh7 cell response to HSV-1 Cgal$^+$ infection before activation of apoptotic pathways, we have analyzed the Huh7 nuclear proteome alterations induced by HSV-1 Cgal$^+$ at 8 hpi, employing two-dimensional-DIGE and tandem mass tag (TMT) isobaric labeling quantitative mass spectrometry using an LTQ-Orbitrap instrument. We provide 62 differential components of the nuclear proteome of Huh7 human hepatoma cells that may regulate host-virus interaction, cell cycle regulation, and RNA homeostasis upon infection highlighting QKI as a cellular factor necessary for an optimal HSV-1 Cgal$^+$ replication.

## EXPERIMENTAL PROCEDURES

*Materials*—The following reagents and materials were used: anti-QKI-5 was kindly provided by Dra. K. Artzt (University of Texas, Austin, Texas), anti-QKI-Pan clone N147/6 (UC Davis/NIH NeuroMab Facility), anti-US11 (27), anti-KDEL, anti-ICP4, anti-ICP27, and anti-$\beta$-actin (Abcam, Cambridge, MA), anti-histone H4 (Millipore, Billerica, MA), anti-p27$^{Kip1}$, anti-p57$^{Kip2}$ (Cell Signaling, Danvers, MA), anti-nectin-1, anti-HDAC-1, anti-HNF$\alpha$, and anti-ICP0 (Santa Cruz Biotechnology, Santa Cruz, CA). Anti-UL42 was kindly provided by Dr. H. Marsden (28). Electrophoresis reagents were purchased from GE Healthcare and trypsin from Promega (Madison, WI).

*Virus Production*—Vero cells were used for propagation and titration of HSV-1 Cgal$^+$. HSV-1 Cgal$^+$ is a replication-competent HSV-1 strain derived from CgalΔ3, which derives from HSV-1 17syn+ with both copies of ICP4 deleted and the insertion of LacZ gene from the intergenic region IGR54. HSV-1 Cgal$^+$ is obtained by repairing both copies of ICP4 (29). Cells were maintained in monolayer with Dulbecco's modified Eagles medium (DMEM) containing 5 to 10% fetal bovine serum and penicillin and streptomycin.

*Culture and treatment of human liver cancer cells*—Huh7 cells (JCRB Genebank, Japan) were cultured in DMEM supplemented with 10% fetal bovine serum, L-glutamine, and penicillin and streptomycin. Huh7 cells ($1 \times 10^6$ or $5 \times 10^6$ cells/dish were used for analytical and proteomic experiments respectively) were infected with HSV-1 Cgal$^+$ at multiplicity of infection (MOI) of 5 plaque forming units (pfu)/cell. After incubation for 1 h at 37 °C, cells were washed and incubated with fresh culture medium under the same conditions during the indicated periods of time. There were no statistically significant differences between control Huh7 cells and Mock-infected Huh7 cells (incubated with a minimum quantity of noninfected Vero cells supernatant). Mock-infected Huh7 cells were used as the reference sample. For QKI silencing, specific small interfering RNAs (siRNA) were used. Transfections were carried out with the DharmaFECT reagent (DharmaFECT 4 Transfection Reagent T-2004–03; Dharmacon Research) according to the instructions of the manufacturer. siRNAs targeting QKI (siQKI: 5′-GGCACCUACAGAGAUGCCAACAU-3′) and control (siGL: 5′-CGUACGCGGAAUACUUCGAUU-3′) were from Dharmacon Research. 36 h after transfection, cells were infected as mentioned above with HSV-1 Cgal$^+$ at MOI of 5 pfu/cell for the indicated periods of time and then processed for appropriate analysis.

*Two-dimensional-DIGE, Imaging, and Mass Spectrometry*—The culture medium was removed after 8 hpi and cells were washed three times with ice cold phosphate-buffered saline (PBS). Subcellular fractionation was performed using the Qproteome Cell Compartment Kit from Qiagen. Nuclear fraction was isolated by differential centrifugation according to the manufacturer's recommendations. After ace-

tone precipitation, protein samples were solubilized in two-dimensional DIGE sample buffer: 7 M urea, 2 M thiourea, 4% 3-[(3-cholamidopropyl) dimethylammonio]-1-propanesulfonate (CHAPS), 30 mM Tris, buffered to pH 8. Protein concentration was determined using the Bradford's assay (Bio-Rad). Then 50 $\mu$g protein were labeled with 400 pmol of CyDye DIGE Fluor minimal dyes (GE Healthcare) and incubated on ice in the dark for 30 min according to the manufacturer's instructions (Cy3, Cy5 for samples and Cy2 for internal control consisting of a mixture composed by equal amounts of protein from all samples). Paired samples were reverse-labeled to prevent potential dye labeling bias. The reaction was stopped by addition of 1 $\mu$l of 10 mM lysine and incubated on ice for 10 min. Samples were up-loaded onto IPG strips, 24 cm, pH 3–11NL (GE Healthcare), and subjected to isoelectric focusing (IEF) in IPGphor™ IEF System (GE Healthcare) according to the manufacturer's recommendations. Upon IEF, strips were incubated in equilibration buffer (50 mM Tris-HCl, pH 8.8, 6 M urea, 30% glycerol, 2% SDS, a trace of bromphenol blue), containing 0.5% dithiotreitol for 15 min and thereafter in the same buffer with 4.5% iodoacetamide for 15 min. For the second dimension, strips were loaded on top of 12.5% polyacrylamide gels (21 $\times$ 24 cm) and run (1W/gel) for 12–14 h until the bromphenol blue dye reached the gel bottom-end. Subsequently, two-dimensional gels were scanned using a Typhoon™ Trio Imager (GE Healthcare) at 100-$\mu$m resolution with $\lambda$ex/$\lambda$em of 488/520, 532/580, and 633/670 nm for Cy2, Cy3, and Cy5 respectively. The photomultiplier tube was set to ensure that the maximum pixel intensity was between 90,000 and 99,000 pixels. Image analysis was performed using DeCyder 6.5 software (GE Healthcare) as described in the user's manual. Three independent experiments were performed. Briefly, the differential in-gel analysis module was used for spot detection, spot volume quantification and volume ratio normalization of different samples in the same gel. Then the biological variation analysis module was used to match protein spots among different gels and to identify protein spots that exhibit significant differences. Manual editing was performed in the biological variation analysis module to ensure that spots were correctly matched between different gels, and to get rid of streaks and speckles. Differential expressed spots were considered for MS analysis when the fold change was larger than 1.2 and the *p* value after *t* test was below 0.05. Preparative gels were run with 350 $\mu$g of protein following the same procedure described above. Proteins were visualized by staining with SYPRO Ruby Protein Gel Stain (Bio-Rad) and images were acquired with a Typhoon™ Trio Imager using $\lambda$ex/$\lambda$em of 532/560 nm. Spots differentially represented were excised manually and gel specimens were processed with a MassPrep station (Waters) as described elsewhere (30). In-gel tryptic digestion was performed with 12.5 ng/$\mu$l trypsin in 50 mM ammonium bicarbonate for 12 h at 37 °C. The resulting peptides were extracted with 5% formic acid (FA), 50% acetonitrile (ACN). Samples were then concentrated in a speed-vac before MS analysis. NanoLC-ESI-MS/MS analysis was performed as described previously (16). Data processing was performed with MassLynx 4.0. Database searching was done with three independent search engines: ProteinLynx Global Server 2.3 (Waters), Phenyx 2.6 (GeneBio), and Mascot Server 2.2 (Matrix Science) against UniprotKB/Swiss-Prot Release 51.6 with 257964 entries (human taxonomy: 15720 entries). Parameters used in Mascot searches were: enzyme, trypsin; variable modifications, carbamidomethylation of cysteine, and oxidation of methionine; maximum missed cleavages, 1; peptide mass tolerance settings/windows was 50 ppm; product mass tolerance, 0.1 Da. Probability *p* of random matches was set to the default value of 0.05.

*Reduction, Alkylation, Digestion, and Labeling with 6-Plex TMT*—Thirty micrograms of nuclear protein extracts from mock and HSV-1 Cgal$^+$-infected Huh7 cells were dissolved in 300 $\mu$l triethylammonium hydrogen carbonate buffer (TEAB) 0.1 M adjusted to pH 8 (Fluka). SDS (Fluka) 1% in water (w:w) was added to obtain a final 0.1% SDS in all samples. Two microliter of 50 mM tris-(2-carboxyethyl)-phosphine hydrochloride (TCEP-HCl) (Sigma) was added. The reaction was performed for 1 h at 60 °C. One $\mu$l of iodoacetamide (Sigma) at 400 mM was then added, and the mixtures were reacted for 30 min in the dark at room temperature. An amount of 10 $\mu$l of freshly prepared trypsin at 0.2 $\mu$g/$\mu$l concentration in TEAB (0.1 M) was added. The digestion was performed overnight at 37 °C. TMT labeling was achieved at room temperature, after addition of 6-plex TMT reagents (0.83 mg) in 40.3 $\mu$l ACN (Sigma-Aldrich). Nuclear extracts from Mock-infected cells (triplicates) were labeled by TMT with reporters at $m/z$ = 126.1, 127.1, and 128.1 and nuclear extracts from HSV-1 Cgal$^+$-Huh7 infected cells by TMT with reporters at $m/z$ = 129.1, 130.1, and 131.1. After 1 h reaction, 8 $\mu$l of 5% hydroxylamine (Sigma) (w/V) was added in each tube and mixed for 15 min. The six samples were pooled in a new tube and dried in a speed-vac for storage at −20 °C. The pooled TMT-labeled sample was ressuspended in 1 ml water:ACN (95:5) 0.1% trifluoroacetic acid (Fluka, Buchs, Switzerland) and cleaned using a OASIS® HLB 1 cc (30 mg) cartridges (Waters, Milford, MA) connected to a vacuum system according to the manufacturer's instructions with slight modifications.

*Off-gel Separation of Pooled TMT-labeled Sample, LC-ESI LTQ-Orbitrap MS/MS Analysis, and Database Search*—After drying, the pooled TMT-labeled sample was dissolved in 1616.4 $\mu$l $H_2O$ with 172.8 $\mu$l glycerol 50% (Agilent Technologies, Santa Clara, CA) and 10.8 $\mu$l of carrier ampholytes IPG buffer pH 3–10 (GE Healthcare). The peptide isoelectric focusing separation was carried out using the 3100 OFFGEL Fractionator (Agilent Technologies). The IPG strip (pH 3–10, 13 cm) (GE Healthcare) was assembled on the off-gel tray and rehydrated for 30 min with a solution of 89.8% $H_2O$, 9.6% glycerol 50%, and 0.6% of carrier ampholytes. The sample was loaded in the 12 off-gel wells. The isoelectric focusing was achieved overnight with a limiting current of 50 $\mu$A and a limit of 20 kV·h before holding the voltage to 500 V. The fractions were collected and their pH was measured (744 pH Meter and Biotrode from Metrohm). The fractions were dried, cleaned with C18 ultramicrospin columns (Harvard Apparatus, Holiston, MA) according to the manufacturer's instructions with slight modifications and dried again. NanoLC-ESI-MS/MS was performed on a LTQ Orbitrap XL (Thermo Electron) equipped with a NanoAcquity system (Waters). Peptides were trapped on a homemade 5 $\mu$m 200 Å Magic C18 AQ (Michrom) 0.1 mm $\times$ 20 mm precolumn and separated on a homemade 5 $\mu$m 100 Å Magic C18 AQ (Michrom) 0.075 mm $\times$ 150 mm column with a gravity-pulled emitter. The nanoLC was run for 85 min using a gradient of water/FA 99.9%/0.1% and ACN/FA 99.9%/0.1% as already described (31) at a flow rate of 220 nL·min$^{-1}$. For MS survey scans, the Orbitrap resolution was set to 60,000 and the ion population was $5 \times 10^5$ with an $m/z$ window from 400 to 2000. A maximum of three precursors was selected for both collision induced-dissociation (CID) in the LTQ and higher-energy C-trap dissociation (HCD) with analysis in the Orbitrap. For MS/MS in the LTQ, the ion population was $1 \times 10^4$ (isolation width of 2 $m/z$), whereas for MS/MS detection in the Orbitrap, it was $2 \times 10^5$ (isolation width of 4 $m/z$), with resolution of 7500, first mass at $m/z$ = 100, and maximum injection time of 750 ms. The normalized collision energies were 35% for CID and 50% for HCD. Dynamic time exclusion was 60 s. Peak lists were generated using an in-house-written Perl script. CID and HCD spectra were merged using a custom-made program (31). The combined mgf file from the nanoLC-ESI-MS/MS analysis of the 12 off-gel fractions was searched against UniProt-Swiss-Prot database (57.4 of 16-Jun-2009, 565634 entries) using Phenyx. *Homo sapiens* taxonomy (40335 entries) was specified. Variable amino acid modifications were oxidized methionine. 6-plex TMT-labeled peptide amino terminus and lysine (+229.1629 Da) and car-

bamidomethylation of cysteines were set as fixed modifications. Trypsin was selected as the enzyme, with one potential missed cleavage. Only one search round was used with selection of "turbo" scoring. The peptide *p* value was $1 \times 10^{-3}$. The protein and peptide scores were set at 5.0, providing a false peptide discovery rate of 2%. The parent ion tolerance was 20 ppm. For all analyses, only proteins matching two different peptide sequences were selected. Reporter-ion intensities were extracted from peak lists using the dedicated Phenyx export. The reporter-ion intensities were corrected according to the isotopic purities of the reporter-ions provided by the manufacturer.

*Bioinformatic Analysis*—TMT data processing was performed using Linear models for microarrays data (32) to find out the peptides that showed significant differential expression between both experimental conditions. For a given protein a score, *p*, was calculated with the *p* values of its corresponding set of identified peptides *S*:

$$p = \frac{-\sum_{i=1}^{|S|} \log_2(p - value_i)}{|S|} \quad \text{(Eq. 1)}$$

To discard inconsistencies, we define a coherence score, *s*, for the set of peptides quantified for a given protein as the average expression similarity of all the possible peptide pairs. The similarity between two peptides *pi* and *pj* is computed as the logarithm of the *p* value obtained using the Spearman rank correlation $p_{cor}$:

$$s = \frac{-\sum_{i=1}^{|S|} \sum_{i=c+1}^{|S|} \log_2(p_{cor(pi,pj)})}{|S|(|S| - 1)/2} \quad \text{(Eq. 2)}$$

The two resulting scores (*p* and *s*) are combined in a unique metric to obtain the ranked list of interesting proteins. The selection of differentially expressed proteins is based on the distribution of this score. All the analysis were performed using R (www.r-project.org) and Bioconductor (www.bioconductor.org) (33). The biological knowledge extraction was carried out through the use of Ingenuity Pathway Analysis (Ingenuity Systems, www.ingenuity.com), which database includes manually curated and fully traceable data derived from literature sources.

*Immunoblotting Analysis*—Equal amounts of protein (15 $\mu$g) were resolved in 12.5% SDS-PAGE gels. Proteins were electrophoretically transferred onto nitrocellulose membranes for 45 min at 120 V. Membranes were probed with primary antibodies at 1:1000 dilution in 5% bovine serum albumin (BSA) or 5% nonfat milk, depending on the primary antibody used. After incubation with the appropriate horseradish peroxidase-conjugated secondary antibody (1:5000), the immunoreactivity was visualized by enhanced chemiluminiscence (Perkin Elmer). Equal loading of the gels was assessed by Ponceau staining and hybridization with a $\beta$-actin specific antibody (Abcam).

*Plaque Assays*—To measure virus production after inhibition of QKI expression, Huh7 cells were treated with control (GL) or QKI siRNAs for 36 h. Cell monolayers were then infected with HSV-1 Cgal$^+$ (MOI = 1pfu/cell). Cells and cell culture supernatants were collected at 16 and 24 hpi. Huh7 cells in six-well plates were inoculated with serial 10-fold dilutions of progeny virus. After a 1 h adsorption period at 37 °C, the inoculum was removed and then overlaid with DMEM supplemented with 1% methylcellulose. After two washes with PBS, plaques were counted and visualized at 72 hpi by fixing and staining the cells with 0.5% crystal violet in water.

*Immunofluorescence Microscopy*—HSV-1 Cgal$^+$-infected or Mock-infected Huh7 cells were grown in chamber slides for the indicated periods of time, washed twice with PBS, fixed for 10 min in 3.7–4% formaldehyde, and made permeable by Triton-X100 5% for 30 min. After blocking in 2% BSA in TBS-0.05% Tween 20 (TBS-T) for 1 h at room temperature, cells were incubated with primary antibodies (rabbit anti-QKI5, dilution 1:1000 or mouse anti-nectin-1, dilution 1:100) overnight at 4 °C. After washing in TBS-T, secondary antibodies, Alexa Fluor 488 goat anti-rabbit (A11008, Molecular Probes, Eugene, OR; dilution 1:200) or Alexa Fluor 568 goat anti-mouse (A11004, Molecular Probes; dilution 1:200) were applied for 60 min at room temperature. Nuclei were counterstained with 4′,6-diamidino-2-phenylindole dihydrochloride (40009, Biotium). Pictures were taken on a Nikon Eclipse E800 microscope equipped with epifluorescence optics. Three independent experiments were performed for the indicated periods of time. The immunofluorescence figures are representative of the overall effects observed under each set of conditions.

## RESULTS

*Two-dimensional-DIGE Analysis of Virally Infected Nuclei*—The capacity of infection and replication of HSV-1 Cgal$^+$ in Huh7 cells were previously tested both *in vitro* and HCC xenograft murine models (15, 16). Nuclear proteome was examined at 8 hpi, when most that 90% of the cells were infected showing minimal morphologic changes (16). Detection of the endoplasmic reticulum marker (KDEL) preferentially in the cytosolic fraction together with detection of histone H4, hepatocyte nuclear factor 1 $\alpha$ (HNF-1$\alpha$) in addition to major histone deacetylase 1 (HDAC-1) location in the nuclear extracts indicated the efficiency of the enrichment procedure (Fig. 1 supporting information). Protein mixtures from nuclear fractions extracted from Mock and HSV-1 Cgal$^+$-Huh7 infected cells (8 hpi) were compared by DIGE analysis, alternating Cy3 and Cy5 labeling to compensate for any differential observation resulting from the chemistry of the fluorescent dyes. Decyder analysis allowed detection and quantification of 2539 spots in the nuclear fraction (Fig. 1). Differences were accepted with *t* test $<0.05$ and a fold-change $>1.2$ (Fig. 2 Supporting information). Differential spots were localized on preparative gels and were identified by nanoLC-ESI-MS/MS after in gel trypsin digestion (see supplemental material for technical details). From the resulting tryptic digests, 32 protein species (16 were up-regulated and 16 down-regulated in nuclear fractions of HSV-1 Cgal$^+$-Huh7 infected cells) corresponding to 24 proteins were unambiguously identified (Table I). Some of the differentially expressed proteins are involved in pre-mRNA splicing. Protein species from Non-POU domain-containing octamer-binding protein, TAR DNA-binding protein 43, hnRNPC, hnRNPA2/B1, hnRNPH3, peptidyl-prolyl cis-trans isomerase E, and Pre-mRNA-splicing factor SPF27 were down-regulated in nuclear fraction of HSV-1 Cgal$^+$-infected Huh7 cells. In contrast, protein species from hnRNPQ and splicing factor arginine/serine-rich 1 were up-regulated in the nucleus of Huh7 infected cells. The expression levels of Non-POU domain-containing octamer-binding protein, TAR DNA-binding protein 43, Pre-mRNA-splicing factor SPF27, and splicing factor arginine/serine-rich 1 genes were measured by RT-PCR in HSV-1 Cgal$^+$-Huh7 infected cells. mRNA

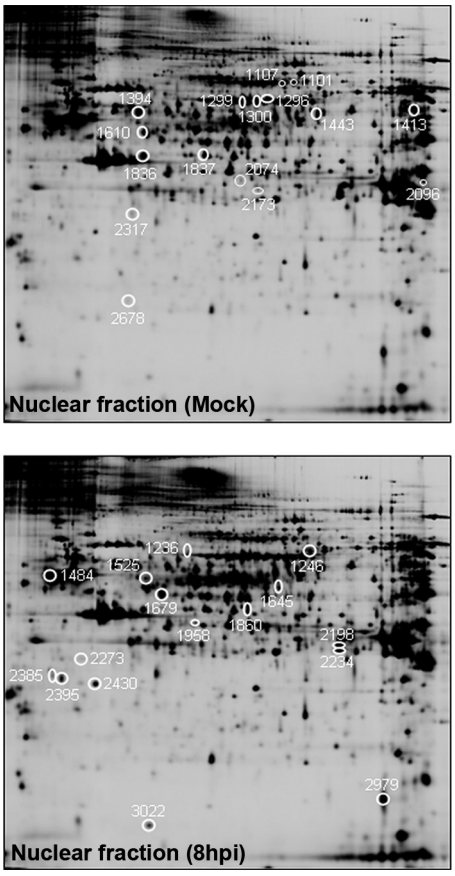


FIG. 1. **Representative two-dimensional images from nuclear proteomes from mock- and HSV-1 Cgal$^{+}$-infected Huh7 cells (8hpi).** White circles indicate those differential spots detected in Huh7-infected nuclei that were subsequently identified by nanoLC-ESI-MS/MS.

levels of these splicing factors were unchanged at 8 hpi (data not shown) indicating that changes detected at protein level may be because of post-translational events. As often appears on two-dimensional gel-based studies, several different spots were identified as products of the same gene. In particular Lamin A-C was identified from six different spots with different pI, where five of them were down-regulated in Huh7-infected cells. These observations suggest that different isoforms or post-translational modifications of this protein might play different roles in the course of HSV-1 Cgal$^{+}$ infection as has been previously demonstrated (34).

*TMT-Analysis of Virus-Infected Cell Nuclei*—A total of 394 proteins were identified and quantified with a minimum of two peptides by TMT analysis comparing virally infected host cell nuclei to uninfected nuclei (see supplemental material). Subcellular location analysis performed with Ingenuity Pathway Analysis software and Human Protein Reference Database (www.hprd.org) revealed that 72.7% of quantified proteins were nuclear proteins suggesting the efficiency of the enrichment procedure (Fig. 3 supplemental material). From the ranked list generated by combination of two scores (*p* and *s*),

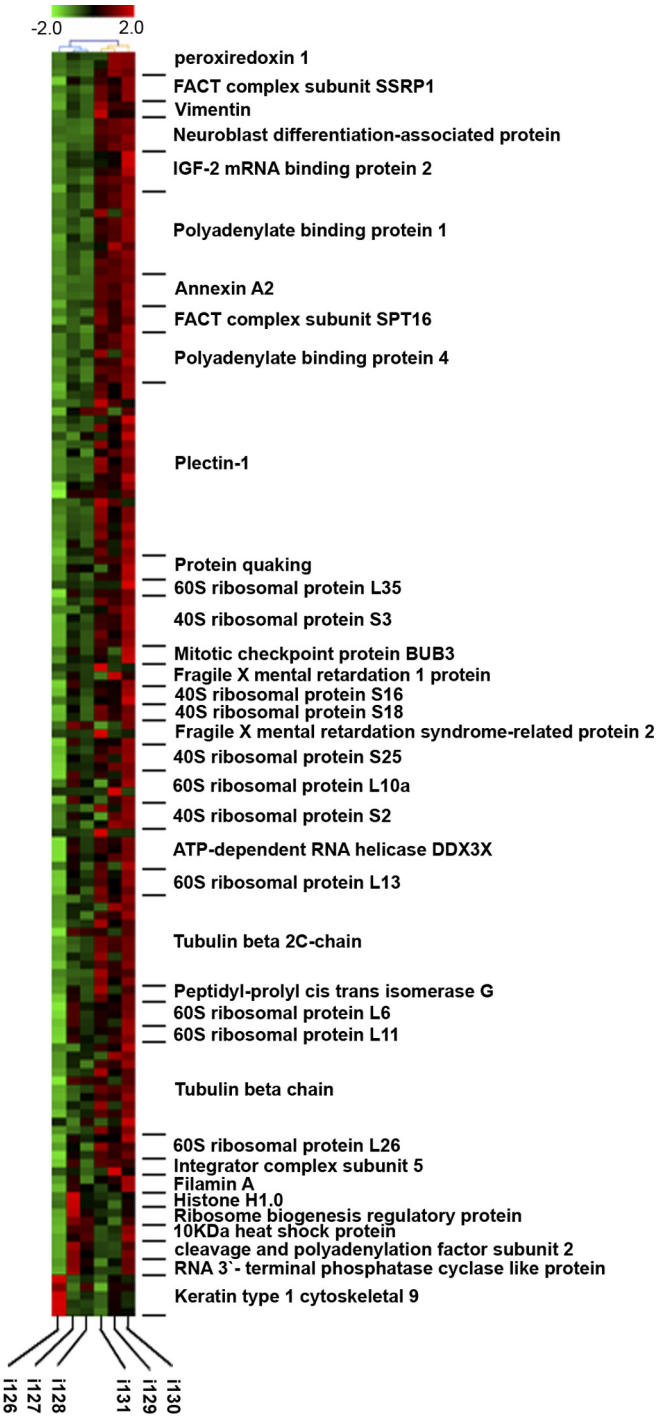


FIG. 2. **Cluster of assigned and quantified peptides.** Intensity values of reporter ions were normalized to the average intensity. Green and red colors indicate values below and above the average intensity value respectively. Ions 126, 127, 128 correspond to mock- infected and 129, 130, and 131 to HSV-1 Cgal$^{+}$-infected cells. Only unique peptides corresponding to differential proteins are represented.

only the upper 20 percentile was considered for further analysis. Moreover, a biological criteria based on subcellular location was used to filter nonnuclear proteins. Finally, 38 pro-

TABLE I
*MS/MS identifications of DIGE differential protein species in infected nuclei*

| Spot | Protein name | C vs 8hpi | | | | | |
|---|---|---|---|---|---|---|---|
| | | Acc. num | Code | T-test | Av. ratio | Peptides | Biological process |
| | **Protein species enriched in the infected nuclei** | | | | | | |
| 1236 | Lamin A-C | P02545 | LMNA | 0,0093 | 1,97 | 9 (6) | Nuclear envelop development |
| 1246 | Heterogeneous Nuclear ribonucleoprotein Q | O60506 | HNRPQ | 0,017 | 1,52 | 5 (3) | Host-virus interaction, mRNA processing, mRNA splicing |
| 1494 | Tubulin b-chain 5 | P07437 | TBB5 | 0,0065 | 1,54 | 22 (16) | Cellular component movement |
| 1525 | Vacuolar ATP syntase subunit B, brain isoform | P21281 | VATB2 | 0,044 | 1,33 | 13 (12) | ATP synthesis |
| 1645 | Septin 11 | Q9NVA2 | SEPT11 | 0,026 | 1,33 | 8 (6) | Cell cycle, cell division |
| 1679 | Actin related protein 3 | P61158 | ARP3 | 0,025 | 1,26 | 16 (12) | Cellular component movement |
| 1860 | $\alpha$-centractin | P61163 | ACTZ | 0,037 | 1,21 | 6 (5) | Vesicle-mediated transport |
| 1958 | Twinfilin-1 | Q12792 | TWF1 | 0,0043 | 1,37 | 5 (4) | Cellular component movement |
| 2198 | Annexin A2 | P07355 | ANXA2 | 0,013 | 1,58 | 4 (3) | Cytoskeletal component movement |
| 2234 | Annexin A2 | P07355 | ANXA2 | 0,0027 | 1,63 | 13 (8) | Cytoskeletal component movement |
| 2273 | Splicing factor, arginine/serine-rich 1 | Q07955 | SFRS1 | 0,0026 | 1,49 | 3 (2) | mRNA procesing, mRNA splicing |
| 2385 | EF-hand domain-containing protein D2 (swiprosin 1) | Q96C19 | EFHD2 | 0,025 | 1,38 | 4 (3) | Calcium ion binding |
| 2395 | EF-hand domain-containing protein D2 (swiprosin 1) | Q96C19 | EFHD2 | 0,0061 | 1,48 | 11 (7) | Calcium ion binding |
| 2430 | Microtubule-associated prot. RP/EB family member 1 | Q15691 | MARE1 | 0,0091 | 1,42 | 9 (7) | Cell cycle, cell division |
| 2979 | Cofilin1 | P23528 | COF1 | 0,0048 | 1,35 | 11 (8) | Response to virus, anti-apoptosis |
| 3022 | Actin-related protein 2/3 complex subunit 5 | O15511 | ARPC5 | 0,014 | 1,59 | 3 (2) | Cellular component movement |
| | **Protein species depleted in the infected nuclei** | | | | | | |
| 1101 | Lamin A–C | P02545 | LMNA | 0,045 | −1,45 | 21 (16) | Nuclear envelop development |
| 1107 | Lamin A–C | P02545 | LMNA | 0,014 | −1,95 | 17 (15) | Nuclear envelop development |
| 1296 | Lamin A–C | P02545 | LMNA | 0,031 | −1,57 | 11 (7) | Nuclear envelop development |
| 1299 | Lamin A–C | P02545 | LMNA | 0,047 | −1,34 | 8 (4) | Nuclear envelop development |
| 1300 | Lamin A–C | P02545 | LMNA | 0,049 | −1,37 | 14 (9) | Nuclear envelop development |
| 1394 | T-complex protein 1 subunit theta | P50990 | TCPQ | 0,015 | −1,28 | 16 (14) | Protein folding |
| 1413 | Non-POU domain-containing octamer-binding protein | Q15233 | NoNO | 0,0033 | −1,22 | 21 (14) | Transcription regulation, mRNA processing, mRNA splicing |
| 1443 | T-complex protein 1 subunit eta | Q99832 | TCPH | 0,039 | −1,31 | 11 (6) | Protein folding |
| 1610 | RuvB like 2 | Q9Y230 | RUVB2 | 0,047 | −1,25 | 23 (18) | DNA recombination, transcription regulation |
| 1836 | BRG1-associated factor 47 | Q12824 | SNF5 | 0,01 | −1,22 | 4 (3) | Host-virus interaction, transcription regulation |
| 1837 | TAR DNA-binding protein 43 | Q13148 | TADBP | 0,0077 | −1,22 | 14 (10) | Transcription regulation, mRNA processing, mRNA splicing |
| 2074 | Heterog. Nuclear ribonucleoprotein C | P07910 | HNRPC | 0,019 | −1,38 | 2 (2) | mRNA processing, mRNA splicing |
| 2096 | Heterog. Nuclear ribonucleoprotein A2/B1 | P22626 | ROA2 | 0,02 | −1,21 | 2 (2) | mRNA processing, mRNA splicing |
| 2173 | Heterogeneous nuclear ribonucleoprotein H3 | P31942 | HNRH3 | 0,0024 | −1,26 | 2 (2) | mRNA processing |
| 2317 | Peptidyl-prolyl cis-trans isomerase E | Q9UNP9 | PPIE | 0,0022 | −1,21 | 5 (3) | mRNA procesing, mRNA splicing |
| 2678 | Pre-mRNA-splicing factor SPF27 | O75934 | SPF27 | 0,031 | −1,29 | 5 (3) | mRNA procesing, mRNA splicing |

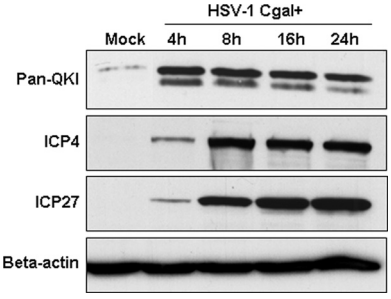


FIG. 3. **mRNA binding QKI protein content during HSV-1 Cgal$^+$ infection.** Steady state levels of cellular QKI protein and viral immediate-early proteins ICP4 and ICP27 in mock- and HSV-1 Cgal$^+$-infected Huh7 cells at 4, 8, 16, and 24 hpi. Equal protein loading was demonstrated using an antibody against $\beta$-actin. Three independent experiments were performed for all experimental conditions. Representative blots are shown.

teins showed significant changes (32 were up-regulated and six down-regulated in nuclear fractions of HSV-1 Cgal$^+$-Huh7 infected cells) (Table II). The estimation of the fold change for each protein was obtained as follows: the mean value of each peptide quantification is calculated for Mock and HSV-1Cgal$^+$ conditions; then the ratios for each reporter are calculated and the log2 of the median of these ratios is considered as the protein fold change. The peptide labeling reproducibility between the different set of biological replicates and the coherence among unique peptides corresponding to the differentially expressed proteins are shown in Fig. 2. One third of the up-regulated proteins correspond to components of 40S and 60S ribosomal subunits and other proteins involved in different steps of translation. Annexin A2 was the unique deregulated protein identified by DIGE and TMT analysis. However, the differential proteins provided by the two strategies showed functional complementarity as both revealed alterations in similar biological processes including host-virus interaction, transcription regulation, mRNA processing, and mRNA splicing allowing a more comprehensive analysis of HSV-1 Cgal$^+$-infected cell nuclei.

TABLE II

*MS/MS identifications of TMT differential proteins in infected nuclei. pvalScore: Summarized p value for each protein based on differential expression of its peptides. coScore, Summarized correlation p value for each protein as a measured of peptide coherence. SumScore, Sum of pvalScore and coScore. FC, Fold change*

| Protein name | Acc. num | Code | pvalScore | coScore | sumScore | FC | Peptides | Biological process |
|---|---|---|---|---|---|---|---|---|
| **Proteins enriched in the infected nuclei** | | | | | | | | |
| Peroxiredoxin 1 | Q06830 | PRDX1 | 16,0399 | 7,1743 | 23,2142 | 1,7464 | 3 | Peroxidase activity |
| FACT complex subunit SSRP1 | Q08945 | SSRP1 | 12,0100 | 8,1994 | 20,2094 | 1,5554 | 3 | DNA replication, transcription regulation |
| Vimentin | P08670 | VIME | 10,1639 | 7,7685 | 17,9324 | 0,6497 | 2 | Host-virus interaction, cellular component movement |
| Neuroblast differentiation-associated protein AHNAK | Q09666 | AHNK | 11,9223 | 5,8670 | 17,7893 | 1,2122 | 4 | Cell differentiation |
| Glycylpeptide N-tetradecanoyltransferase 1 | P30419 | NMT1 | 7,2050 | 9,4919 | 16,6969 | 0,4003 | 2 | Metabolism |
| Insulin-like growth factor 2 mRNA-binding protein 2 | Q9Y6M1 | IF2B2 | 8,9190 | 7,7685 | 16,6876 | 0,9958 | 3 | Translation regulation |
| Polyadenylate-binding protein 1 | P11940 | PABP1 | 9,6184 | 6,6451 | 16,2634 | 1,1670 | 10 | mRNA processing, mRNA splicing |
| Annexin A2 | P07355 | ANXA2 | 8,9164 | 7,0965 | 16,0129 | 0,7852 | 4 | Calcium ion binding |
| FACT complex subunit SPT16 | Q9Y5B9 | SP16 | 10,1472 | 4,9612 | 15,1084 | 0,5962 | 3 | DNA replication, transcription regulation |
| Polyadenylate-binding protein 4 | Q13310 | PABP4 | 8,6813 | 5,9284 | 14,6097 | 1,0341 | 6 | RNA processing |
| Plectin-1 | Q15149 | PLEC1 | 8,7706 | 5,6492 | 14,4198 | 1,0740 | 21 | Hemidesmosome assembly |
| Protein quaking, isoform 7 (***) | Q96PU8 | QKI | 6,5499 | 7,1009 | 13,6508 | 0,6695 | 3 | mRNA processing, mRNA splicing, mRNA translation |
| 60S ribosomal protein L35 | P42766 | RL35 | 6,6102 | 6,9069 | 13,5171 | 0,2687 | 2 | Translational elongation |
| 40S ribosomal protein S3 | P23396 | RS3 | 3,8546 | 8,4352 | 12,2898 | 0,4632 | 6 | Translational elongation |
| Mitotic checkpoint protein BUB3 | O43684 | BUB3 | 2,7463 | 9,4919 | 12,2381 | 0,1991 | 2 | Cell cycle, cell division |
| Fragile X mental retardation 1 protein | Q06787 | FMR1 | 8,6019 | 3,1510 | 11,7529 | 0,4786 | 3 | mRNA transport |
| 40S ribosomal protein S16 | P62249 | RS16 | 3,2306 | 8,4579 | 11,6885 | 0,4440 | 2 | Translational elongation |
| 40S ribosomal protein S18 | P62269 | RS18 | 3,9675 | 6,9147 | 10,8822 | 0,5440 | 2 | Translational elongation |
| Fragile X mental retardation syndrome-related protein 2 | P51116 | FXR2 | 7,6701 | 3,0899 | 10,7600 | 0,4486 | 3 | mRNA transport |
| 40S ribosomal protein S25 | P62851 | RS25 | 3,7230 | 6,7353 | 10,4583 | 0,4746 | 3 | Translational elongation |
| 60S ribosomal protein L10a | P62906 | RL10A | 7,5682 | 2,8292 | 10,3974 | 0,0916 | 4 | RNA processing |
| 40S ribosomal protein S2 | P15880 | RS2 | 3,7454 | 6,5032 | 10,2486 | 0,4844 | 4 | Translational elongation |
| ATP-dependent RNA helicase DDX3X | O00571 | DDX3X | 3,8305 | 6,0674 | 9,8979 | 0,3152 | 5 | Host-virus interaction |
| 60S ribosomal protein L13 | P26373 | RL13 | 3,1808 | 6,5736 | 9,7544 | 0,3718 | 3 | Translational elongation |
| Tubulin beta-2C chain | P68371 | TBB2C | 4,3227 | 4,9590 | 9,2817 | 0,5401 | 11 | Cellular component movement |
| Peptidyl-prolyl cis-trans isomerase G | Q13427 | PPIG | 2,2971 | 6,9069 | 9,2040 | 0,4412 | 2 | RNA splicing, protein folding |
| 60S ribosomal protein L6 | Q02878 | RL6 | 1,3499 | 7,7685 | 9,1184 | 0,1717 | 3 | Transcription regulation, translational elongation |
| 60S ribosomal protein L11 | P62913 | RL11 | 3,5067 | 5,5591 | 9,0658 | 0,2563 | 2 | Translational elongation, rRNA processing |
| Tubulin beta chain | P07437 | TBB5 | 3,9414 | 5,0628 | 9,0042 | 0,3657 | 11 | Cellular component movement |
| 60S ribosomal protein L26 | P61254 | RL26 | 2,9984 | 5,8199 | 8,8183 | 0,2511 | 3 | Translational elongation |
| Integrator complex subunit 5 | Q6P9B9 | INT5 | 6,0501 | 2,7504 | 8,8005 | 0,5586 | 2 | Small nuclear RNAs (snRNA) U1 and U2 transcription |
| Filamin-A | P21333 | FLNA | 2,0689 | 6,9069 | 8,9758 | 0,2458 | 2 | Actin cytoskeleton reorganization |
| **Proteins depleted in the infected nuclei** | | | | | | | | |
| Histone H1.0 | P07305 | H10 | 0,5559 | 9,4919 | 10,0478 | −0,0634 | 2 | Nucleosome assembly |
| Ribosome biogenesis regulatory protein homolog | Q15050 | RRS1 | 0,4226 | 9,4919 | 9,9144 | −0,1703 | 2 | Ribosome biogenesis |
| 10 kDa heat shock protein | P61604 | CH10 | 0,3955 | 9,4919 | 9,8874 | −0,2388 | 2 | Protein folding |
| Cleavage and polyadenylation specificity factor subunit 2 | Q9P2I0 | CPSF2 | 0,1765 | 9,4919 | 9,6683 | −0,2210 | 2 | mRNA processing |
| RNA 3′-terminal phosphate cyclase-like protein | Q9Y2P8 | RCL1 | 0,1194 | 9,4919 | 9,6113 | −0,1564 | 2 | Ribosome biogenesis |
| Keratin, type I cytoskeletal 9 | P35527 | K1C9 | 2,7156 | 6,2839 | 8,9996 | −0,0743 | 5 | Intermediate filament elongation |

*Increase of Quaking RNA Binding Protein During HSV-1 Cgal$^+$ Infection*—QKI was one of the most interesting nuclear alterations induced by HSV-1 Cgal$^+$ infection as revealed by TMT analysis. QKI is involved in the regulation of mRNA stability, nuclear retention, RNA transport, and translational modulation through interaction with the Quaking Response Element (35). Although conventional data processing suggested QKI-7 as the modified isoform (Table II), the three corresponding peptides used for protein identification and quantification (peptides from residue 26 to 44; 85–102; 177–

192) belong to the STAR (Signal Transduction Activator of RNA metabolism) domain of QKI, which is conserved between the different alternatively splice variants of *qkI* gene. To validate the potential up-regulation of QKI protein content in infected Huh7 cells, we used an anti-QKI-Pan antibody that recognizes the three major QKI isoforms (QKI-5, QKI-6, and QKI-7). As shown in Fig. 3, Mock-infected Huh7 cells expresses low levels of QKI that peak at 4 hpi leading to a time dependent decrease during the infection. Interestingly, viral immediate-early genes such as ICP4 and ICP27 are translated when QKI protein peaks 4hpi (Fig. 3).

*Inhibition of QKI Expression Results in Reduction of Viral Protein Content and Viral Yield in Huh7 Cells*—Based on the correlation between the up-regulation of QKI and the expression of viral immediate-early proteins in Huh7-infected cells, we hypothesize that QKI protein could be one of the cellular proteins that plays a direct role in viral replication. To test this possibility, we carried out experiments using siRNA strategy to knockdown QKI expression. A reduction of 50% in QKI protein levels was observed 36 h post-transfection in siQKI cells with respect to control siGL cells (supplemental material; Fig. 4) without observing any alterations in Huh7 cell morphology and cell viability until 72 h post-transfection. To determine whether QKI depletion can affect the efficiency of viral replication, Huh7 cells were submitted to HSV-1 Cgal$^{+}$ infection (MOI = 5 pfu/cell) 36 h post-transfection with the siRNAs. First, we monitored the capacity of infection of HSV-1 Cgal$^{+}$ in siGL and siQKI Huh7 cells (36 h post-transfection) by X-Gal staining at 4, and 8 hpi as described previously (16). No differences in $\beta$-galactosidase transgene expression were observed in siGL and siQKI infected-Huh7 cells (supplemental material; Fig. 5). These data point out that HSV-1 Cgal$^{+}$ infectivity is not hampered in cells where QKI expression is inhibited also suggesting that QKI is not essential for viral entry. The effect on viral replication was determined 4, 8, and 16 hpi by western-blot using specific antibodies against immediate-early viral proteins. As shown in Fig. 4, QKI protein expression was transiently increased 4–8hpi in siGL-infected cells indicating that transfection with nonspecific siRNA has no significant consequence on QKI expression pattern upon infection. We observed that the levels of ICP27 and ICP4 proteins were decreased in cells transfected with QKI siRNA at 4, and 8 hpi with respect to siGL Huh7-infected cells. Although ICP4 levels were still failing in siQKI Huh7-infected cells, ICP27 levels were not significantly modified between both conditions at 16 hpi (Fig. 4*A*). Moreover ICP0 protein was also down-regulated at 8, and 16 hpi in siQKI Huh7-infected cells (Fig. 4*A*). These results indicate that immediate-early viral functions are partially delayed in cells where QKI expression is down-regulated. To determine whether the observed QKI dependent alteration was specific of immediate-early viral factors, the amounts of some early and late viral proteins were tracked by Western blot analysis. The expression of polymerase accessory viral protein UL42 (early gene) and the tegument protein US11 (late gene) was also hampered in siQKI Huh7-infected cells respect to control siGL Huh7-infected cells at 8 hpi (Fig. 4*B*). Subsequent experiments were performed to analyze the effect of repression of QKI expression on the amounts of progeny virus produced in Huh7 cells for 16 and 24 h. Although viral yield significantly increased from 16 hpi to 24 hpi in siGL-infected cells, there was a block in the production of viral particles in siQKI-infected cells during the infection (Fig. 4*C*). Although no differences were detected between siGL and siQKI cells at 16 hpi, a 40% reduction in virus yield was detected in siQKI cells infected

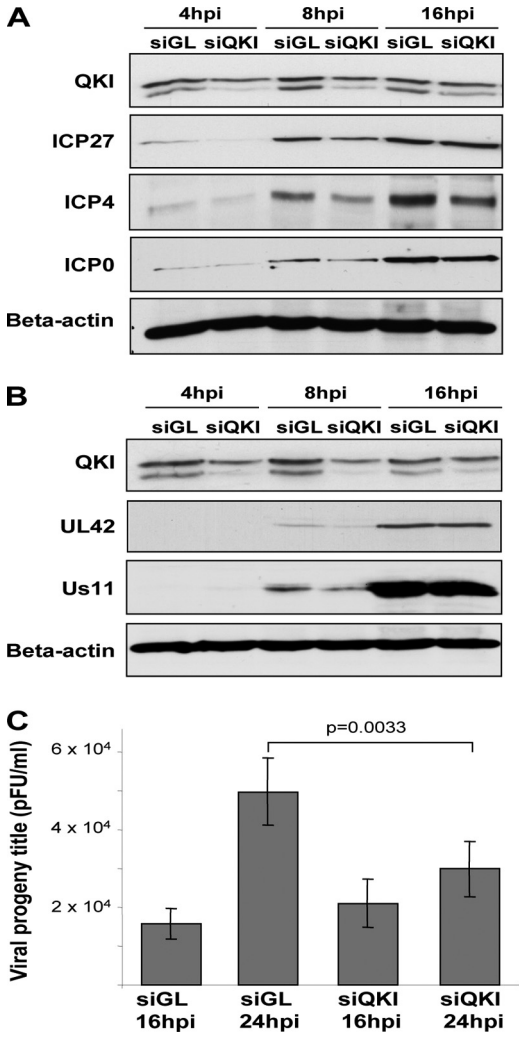


FIG. 4. **Silencing of QKI slows down viral protein expression.** Huh7 cells were transfected with control siGL or siQKI during 36 h and synchronously infected with HSV-1 Cgal$^{+}$. Cellular lysates were harvested and analyzed for the expression of viral proteins at 4, 8, and 16 hpi. *A*, Steady-state levels of immediate-early viral proteins ICP4, ICP27, and ICP0 in siGL and siQKI cells. *B*, Steady-state levels of early (UL42) and late (US11) viral proteins. Blots are representative of results obtained in 3 independent experiments. *C*, Estimation of the amounts of progeny viruses from siGL and siQKI-infected cells and cell culture supernatants harvested after 16 or 24 hpi at 37 °C as indicated. Plaque assays were performed in triplicates for each condition.

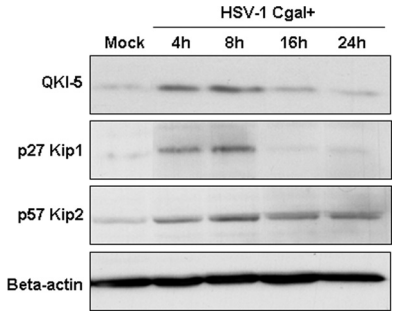


FIG. 5. **QKI-5 and cell-cycle regulators protein levels in Huh7 cells upon HSV-1 Cgal$^+$ infection.** HSV-1 Cgal$^+$ induces a transient increase in QKI-5 levels in parallel with that of its target p27$^{Kip1}$. In contrast, p57$^{Kip2}$ levels were maintained late in infection. A representative Western blot from three independent experiments is shown. Equal protein loading was ensured using an antibody against $\beta$-actin.

with HSV-1 Cgal$^+$ (MOI = 1 pfu/ml) compared with siGL-infected cells at 24 hpi (Fig. 4*C*). All this data demonstrate the pivotal role of QKI in the regulation of the expression of essential proteins mediating the early phases of HSV-1 Cgal$^+$ replication.

*HSV-1 Cgal$^+$ Increases QKI-5 Isoform Levels in Human Hepatoma Cells*—As TMT-based analysis detected an increase in a QKI isoform in the nucleus of Huh7-infected cells and QKI-5 isoform (QKI-5) presents a nuclear localization signal (36), subsequent experiments were performed to check the steady-state protein levels of QKI-5 in Huh7-infected cells using a specific antibody against a C-terminal peptide from QKI-5. The specificity of the QKI-5 antibody was assessed by Western blot and immunofluorescence analysis (supplemental material; Fig. 6). QKI-5 protein content was increased until 4 hpi maintaining its levels until 8 hpi to decrease late in infection in infected-human hepatoma cells (Fig. 5). At a functional level, QKI isoforms bind and stabilizes the mRNA encoding the cyclin-dependent kinase (CDK)-inhibitor p27$^{Kip1}$, leading to an increased protein accumulation (37, 38). To evaluate whether QKI protein was maintaining its well-known function during the infection, additional experiments were performed to investigate one of its targets, p27$^{Kip1}$. As shown in Fig. 5, p27$^{Kip1}$ displayed a transient increase during viral infection, in parallel with QKI-5 expression, suggesting that its mRNA may be stabilized by QKI-5 during the infection. Another negative regulator of the G1-S phase transition, that is functionally and structurally related to p27$^{Kip1}$ is p57$^{Kip2}$ (39). As shown in Fig. 5, p57$^{Kip2}$ showed a transient increase upon infection maintaining high levels onwards 8 hpi. The transient increase in p27$^{Kip1}$ and p57$^{Kip2}$ levels (Fig. 5) points out a partial blockage of the cell-cycle in HSV-1 Cgal$^+$-infected Huh7 cells at 4–8 hpi.

*QKI-5 Isoform Localizes in Different Intracellular Compartments During HSV-1 Cgal$^+$ Infection*—As QKI-5 has been described as a nucleo-cytoplasmic shuttle protein (36, 40), additional experiments were carried out to study the subcellular localization of QKI-5 during HSV-1 Cgal$^+$ infection using the same antibody mentioned above. Immunofluorescent staining of Mock-infected Huh7 cells revealed that QKI-5 showed a diffuse staining throughout the nucleus (excluded from nucleoli) forming 2–3 aggregate structures at perinuclear level in Mock-infected Huh7 cells (Fig. 6, *upper panel*) likely suggesting association with nuclear bodies, which identification still remain elusive. Between 4 and 8hpi, while still nuclear, the aggregate structures were dispersed and redistributed in more punctuate dots throughout the nucleus (Fig. 6, *middle panel*). By 16–24 hpi, QKI-5 is localized in the cytoplasm forming a granular-type pattern, with low level of nuclear fluorescence (Fig. 6, *lower panel*), indicating that QKI-5 shuttles from the nucleus to the cytosol in Huh7 cells in response to HSV-1 Cgal$^+$ infection. Strong linear staining were also observed in several cell-to-cell contact regions at 16–24hpi (Fig. 6, *lower panel*). As nectin-1 is a specific cellular receptor for HSV-1 localized at cell contact areas in infected cells (41), colocalization experiments were undertaken. Nectin-1 distribution revealed a dotted pattern at the cell surface of infected-Huh7 cells 16 and 24 hpi (Fig. 7). Interestingly, nectin-1 staining co-localized with QKI-5 in cell-to-cell contact regions of some infected cells (Fig. 7), suggesting that QKI-5 may participate in the cell fusion phenomena induced by HSV-1 Cgal$^+$ infection.

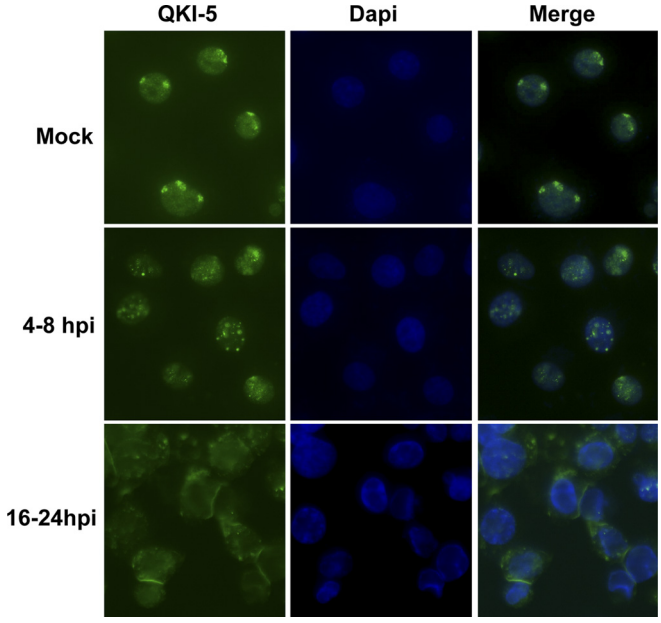


FIG. 6. **Localization of QKI-5 in human hepatoma cells during HSV-1 Cgal$^+$ infection.** The cellular distribution of QKI-5 in control mock-infected Huh7 cells (*upper panel*), and in cells infected for 4–8 hpi (*middle panel*) and 16–24 hpi (*lower panel*) Huh7 infected cells was investigated by immunofluorescence microscopy analysis. The initial diffuse nuclear distribution showing 2–3 aggregate structures switches 4–8 hpi to a dotted nuclear pattern and to display a cytosolic location 16–24 hpi. Representative images are shown.

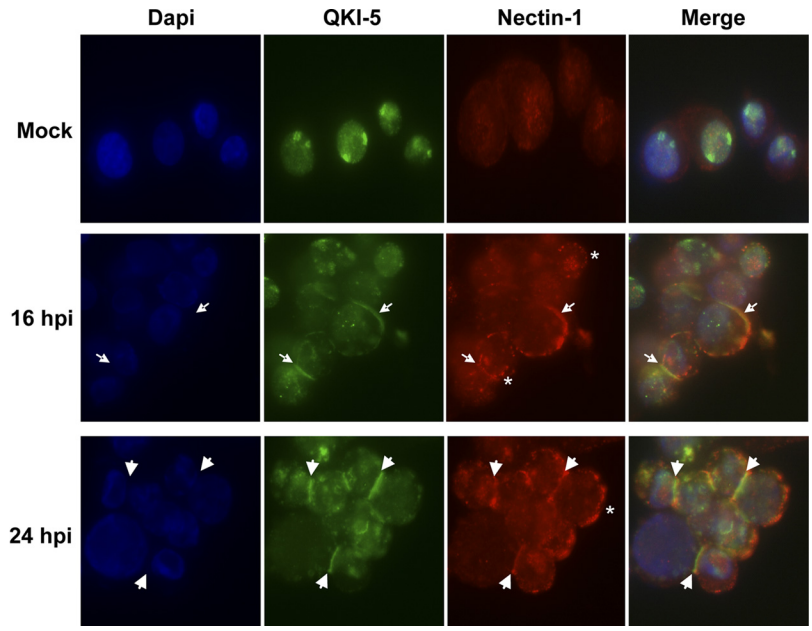


FIG. 7. **Co-localization of nectin-1 and QKI-5 in human hepatoma cells infected with HSV-Cgal$^{+}$ vector.** Cellular distribution of nectin-1 and QKI-5 was analyzed by immunofluorescence in control mock-infected Huh7 cells (*upper panel*), and in cells infected for 16 h (*middle panel*) and 24 h (*lower panel*). Nectin-1 staining shows a dotted pattern likely in association with the plasma membrane (asterisks), colocalizing with QKI-5 in cell to cell contact areas (*arrows*). Representative images are shown. As shown in the figure, the antibody to nectin-1 showed some unspecific cross-reactivity with the nucleus.

## DISCUSSION

HSV-1 is one of the most promising viral platforms for the development on oncolytic vectors that can target, multiply in, and eradicate hepatoma cells (42), but the intermediates mediating the tumoral cell response must be elucidated to promote the development of more efficient and selective HSV-1-based vectors. By comparative cytosolic and microsomal proteome analysis we have previously identified deregulation of central intermediates targeted by HSV-1 Cgal$^{+}$ resulting in the impairment of apoptosis and cell survival pathways in human hepatoma cells (16). In this report, we have applied two different labeling proteomic approaches, two-dimensional-DIGE and TMT to analyze changes in the nuclear proteome composition that arise in infected-human hepatoma cells before caspase activation (16). The application of two different proteomic strategies was particularly useful in obtaining complementary information; accordingly, only one protein was found to be common to both experimental approaches. The complementary data result from the differences in sample preparation and analytical methods used by the two proteomic workflows. two-dimensional-DIGE is a gel-based method that labels samples at the protein level (43) and TMT is a liquid-based method that labels samples at the peptide level (31). Although DIGE separates only soluble proteins included in a pH range of 3 to 11 and a determined molecular weight, TMT can identify proteins outside these ranges. Moreover, DIGE is able to detect differential expression of post-translationally modified proteins as well as different isoforms of proteins by resolving spots at different p*I* and molecular weight. However, these isoforms may not be distinguished with TMT approach, because labeling is completed at the peptide level and most peptide sequences are identical among a group of isoforms. In addition, proteins with extreme isoelectric points, large molecular weights, low solubility (hydrophobic proteins) and low copy numbers are poorly represented in Two-dimensional-DIGE experiments. On the other hand, TMT technique could lead to peptide loss because of TCEP used for protein reduction (44, 45), interaction between peptides and gel matrix during the off-gel electrophoresis, and peptide tagging (46). Differential proteins revealed by both methods appear to be complementary in mediating parallel biological functions in HSV-1 Cgal$^{+}$ -infected human hepatoma cells (Fig. 8), such as host-virus interaction, cell-cycle regulation, transcription regulation, mRNA processing, and mRNA splicing. Despite the well-known protein synthesis shutoff inherent to HSV-1 infection, most of the differentially expressed proteins reported in this study were up-regulated. As it has been postulated, those proteins that continue to be efficiently synthesized upon HSV-1 infection could play a major role in determining the outcome of infection (12).

QKI is involved in the regulation of mRNA stability, nuclear retention, RNA transport, and translational modulation through interaction with Quaking Response Element located in the UTR of target mRNAs (47). QKI isoforms regulate aspects of RNA metabolism in several cellular processes including myelination, cell fate determination, embryogenesis, apoptosis, and protein translation (48). The essential function of QKI in cell biology is further suggested by its widespread expression in different cell types (36, 38, 48) and by the finding that total ablation of QKI in mice results in early embryonic lethality (49). Furthermore, evidence of alterations of QKI expression in cancer tissues (38, 48) together with the critical regulator of p27$^{Kip1}$, suggests that abnormal levels of this protein may contribute to deregulation of cell growth. We have shown that QKI protein and its target cyclin-dependent kinase inhibitor p27$^{Kip1}$ (CDKN1B) (37, 38) transiently increase

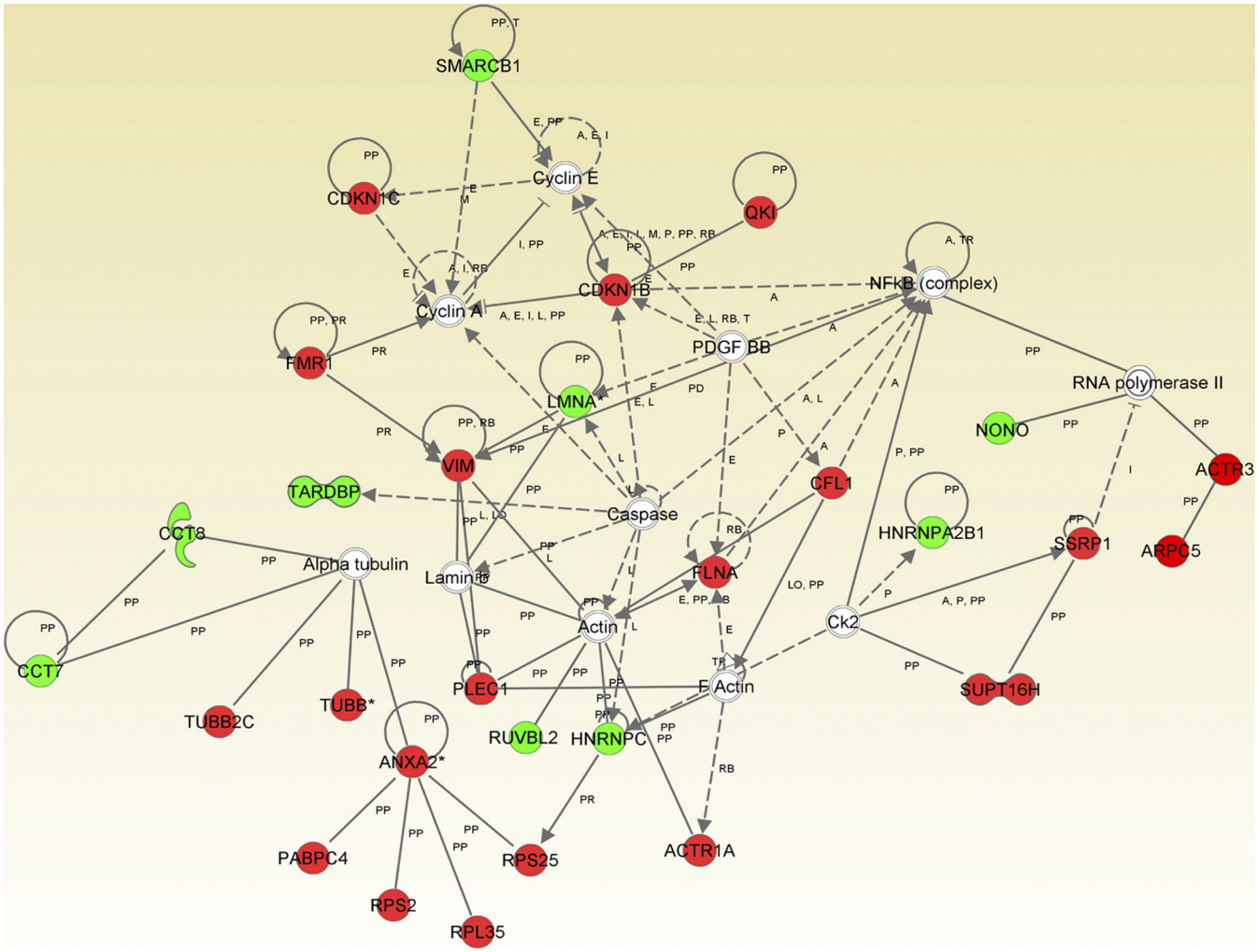


FIG. 8. **Functional clustering of differentially expressed nuclear proteins in HSV-1 Cgal$^{+}$-infected Huh7 cells (8hpi).** Proteomic and functional data were grouped according to Ingenuity interaction parameters. The selected proteins are represented by different symbols (red and green are up- and down-regulated in infected Huh7 cells, respectively) according to their functional classification (see legend in Supporting Information). Complete protein names are listed in Tables I and II. Nodes are displayed using various shapes that represent the functional class of the protein: concentric circles represent a group or complex; double circles stand for transcription regulators; helix shapes represent enzymes; and circles represent other actors. The nodes are linked by specific connectors according to the type of interaction between the nodes. Solid lines indicate direct interactions between nodes and dashed lines indicate indirect interactions (A, Activation/deactivation; RB, Regulation of binding; PR, Protein-mRNA binding; PP, Protein-Protein binding; B, binding; E, expression; I, inhibition; L, Proteolysis; M, Biochemical Modification; P, Phosphorylation/Desphosphorylation; T, Transcription; LO, Localization).

their levels in a parallel way at early times of HSV-1 Cgal$^{+}$ infection, likely blocking the G1-S phase transition of the cell-cycle. These observations are in agreement with the proliferation blockage and tumorigenesis ability inhibition that occur when QKI is overexpressed (38, 50). However, the late fall in p27$^{Kip1}$ protein levels in infected-human hepatoma cells might result from the HSV-1 virion host shutoff (8). In contrast, cyclin-dependent kinase inhibitor p57$^{Kip2}$ (CDKN1C) maintains its levels in infected-human hepatoma cells late in infection. p57$^{Kip2}$ promotes cell death via the mitochondrial apoptotic pathway with caspase 3 activation in cancer cells (51) suggesting that p57$^{Kip2}$ may mediate the multi-factorial impairment of proapoptotic factors previously described in HSV-1 Cgal$^{+}$-infected human hepatoma cells (16). The QKI up-regulation occurs during the immediate-early stage of HSV-1 infection in human hepatoma cells. Depletion of QKI did not compromised the entry and replication of HSV-1 virions, as evidenced by the expression of the reporter gene $\beta$-galactosidase. However, analysis of steady-state levels of viral proteins representing each of the three major kinetic classes (IE, E, and L genes) indicates that QKI knock-down induces a clear delay in viral protein synthesis. Besides the existing cooperativity between IE proteins regarding intracellular localization (52) and the interdependence for assembly into viral particles (53), IE proteins are continuously required for the synthesis of all the virally encoded proteins. ICP0 acts

as a transactivator of all classes of HSV-1 genes (54, 55, 56, 57). ICP4 is absolutely required for progression beyond the immediate-early phase of gene expression because of its role as a transcriptional activator of early and late (58, 59, 60). The IE protein ICP27 is also required for early DNA replication genes such as UL42 (61, 62) and also for transcription of viral late genes (61, 63). In view of our results, QKI is part of the cellular machinery necessary for an optimal HSV-1 Cgal$^+$ replication as is also the case for human immunodeficiency virus (HIV) (64).

The mammalian *qkI* gene undergoes a complex pattern of alternative splicing and generates at least three major transcripts of 5, 6, and 7 kb, corresponding to QKI-5, QKI-6, and QKI-7 isoforms (48). QKI-6 and QKI-7 are mainly cytoplasmic isoforms whereas the unique sequence located at the C terminus of the QKI-5 isoform possesses a noncanonical nuclear localization signal (48). Moreover, the RNA binding domain is important for the localization of QKI-5 in the nucleoplasm (36). By immunofluorescence microscopy analysis, QKI-5 showed a diffuse staining throughout the nucleus as has been previously reported in neuronal and epithelial HeLa cells (36, 48). In contrast to HeLa cells, QKI-5 forms 2–3 aggregate structures at perinuclear level in human hepatoma cells. Furthermore, we showed that HSV-1 Cgal$^+$ infection induces an early QKI-5 nuclear spreading forming dotted structures that may be promyelocytic leukemia protein bodies or Virus-Induced Chaperone-Enriched domains, previously related with HSV-1 replication (65, 66). After 16 hpi, HSV-1 Cgal$^+$ induces QKI-5 nuclear-cytoplasmic shuttling, an event previously shown during normal embryonic neuronal cell fate decision (40). This nuclear-cytoplasmic shuttling may be mediated by post-translational modifications, already described for this protein, such as phosphorylation (67) or arginine methylation (68) as previously confirmed for Sam68, member of the STAR family that shares the heterogeneous ribonucleoprotein K homologue domain (KH *domain*) with QKI-5 (68). The mechanisms promoting QKI-5 shuttling and the biological implications of its cytoplasmic localization remain unclear. Concerning the first issue, active transcription mediated by RNA polymerase II is necessary for nuclear retention of QKI-5 (36, 69, 70). According to this mechanism, QKI-5 shuttling may be a consequence of changes in the activation state of RNA polymerase II that occur during HSV-1 infection (71). The function of cytosolic QKI-5 might be related with the transport and processing of specific cellular RNAs (35) in a process integrating other QKI isoforms (36). Late in infection, QKI-5 is channeled to the cell surface where it colocalizes with nectin-1 in cell-to-cell contact areas in some infected cells. Nectin-1 displayed a dotted distribution at the cell surface at 16 and 24 hpi in human hepatoma cells, as previously reported in HSV-1-infected melanoma cells (41). Nectin-1 belongs to the $Ca^{2+}$-independent cell adhesion proteins of the immunoglobulin superfamily (72) found at adherens junctions (73). Although nectin-1 is considered to be the most important receptor for HSV-1 entry (74), it also serves as cell-cell spread mediator of HSV-1 (75). Cell-cell spread occurs when cell-associated virus propagates to adjacent cells through areas of cell contact by molecular events that are not completely known (76). Our co-localization studies suggest that QKI-5 may be involved in the nectin-1-dependent events occurring at the plasma membrane during cell-cell spread.In summary, we provide a broad analysis of the nuclear proteome of human hepatoma Huh7 cells upon HSV-1 Cgal$^+$ infection using two distinct proteomic strategies. Complementary data sets were generated and integrated on a single functional interpretation to uncover novel response mechanisms triggered by HSV-1 Cgal$^+$ vector in human hepatoma cells. We have demonstrated that early QKI protein up-regulation is necessary for optimal viral protein translation in human hepatoma cells. Moreover, the time-dependent re-distribution of specific QKI-5 isoform in Huh7-infected cells may take part in the cell fusion events observed late in infection.

*Acknowledgments*—The technical assistance of Carmen Miqueo, Manuela Molina, and Coline Biollay is acknowledged. We thank the Morphology Core Facility at CIMA for immunofluorescence analysis. We also thank Proteome Science plc for providing TMT reagents.

* This work was supported by: the agreement between FIMA and the "UTE project CIMA"; grants Plan Nacional I+D+I SAF2008–0154 from Ministerio de Ciencia e Innovación to FJC; grant STREP FP6–2004-LIFESCIHEALTH-5 018649 (THOVLEN) from the 6th framework program of the UE to FJC; ISCIII-RETIC RD06/0020 to MAA and FJC. VSQ had fellowships from FIMA and Boehringer Ingelheim. The Proteomics Core Facility at CIMA is member of the National Institute of Proteomics Facilities, ProteoRed.

S This article contains supplemental material.

** To whom correspondence should be addressed: Division of Hepatology and Gene Therapy. CIMA, Faculty of Medicine, University of Navarra, 31008 Pamplona, Spain. Tel.: 34-948-194700; Fax: 34-948-194717; E-mail: esantamar@unav.es.

¶ Both author's share senior authorship.

REFERENCES

1. Clements, J. B., Watson, R. J., and Wilkie, N. M. (1977) Temporal regulation of herpes simplex virus type 1 transcription: location of transcripts on the viral genome. *Cell* **12,** 275–285
2. Phelan, A., and Barklie, Clements, J. (1997) Functional Domains within the Nucleus of a Cell Infected with HSV-1. *Rev. Med. Virol.* **7,** 229–237
3. Antrobus, R., Grant, K., Gangadharan, B., Chittenden, D., Everett, R. D., Zitzmann, N., and Boutell, C. (2009) Proteomic analysis of cells in the early stages of herpes simplex virus type-1 infection reveals widespread changes in the host cell proteome. *Proteomics* **9,** 3913–3927
4. Döhner, K., Radtke, K., Schmidt, S., and Sodeik, B. (2006) Eclipse phase of herpes simplex virus type 1 infection: Efficient dynein-mediated capsid transport without the small capsid protein VP26. *J. Virol.* **80,** 8211–8224
5. Honess, R. W., and Roizman, B. (1974) Regulation of herpesvirus macromolecular synthesis. I. Cascade regulation of the synthesis of three groups of viral proteins. *J. Virol.* **14,** 8–19
6. Honess, R. W., and Roizman, B. (1975) Regulation of herpesvirus macromolecular synthesis: sequential transition of polypeptide synthesis requires functional viral polypeptides. *Proc. Natl. Acad. Sci. U.S.A.* **72,** 1276–1280
7. Taylor, T. J., Brockman, M. A., McNamee, E. E., and Knipe, D. M. (2002) Herpes simplex virus. *Front Biosci.* **7,** d752–764
8. Kwong, A. D., Kruper, J. A., and Frenkel, N. (1988) Herpes simplex virus virion host shutoff function. *J. Virol.* **62,** 912–921

9. Sydiskis, R. J., and Roizman, B. (1967) The disaggregation of host polyribosomes in productive and abortive infection with herpes simplex virus. *Virology* **32,** 678–686
10. Hardy, W. R., and Sandri-Goldin, R. M. (1994) Herpes simplex virus inhibits host cell splicing, and regulatory protein ICP27 is required for this effect. *J. Virol.* **68,** 7790–7799
11. Rice, S. A., Long, M. C., Lam, V., and Spencer, C. A. (1994) RNA polymerase II is aberrantly phosphorylated and localized to viral replication compartments following herpes simplex virus infection. *J. Virol.* **68,** 988–1001
12. Callé, A., Ugrinova, I., Epstein, A. L., Bouvet, P., Diaz, J. J., and Greco, A. (2008) Nucleolin is required for an efficient herpes simplex virus type 1 infection. *J. Virol.* **82,** 4762–4773
13. Greco, A., Bienvenut, W., Sanchez, J. C., Kindbeiter, K., Hochstrasser, D., Madjar, J. J., and Diaz, J. J. (2001) Identification of ribosome-associated viral and cellular basic proteins during the course of infection with herpes simplex virus type 1. *Proteomics* **1,** 545–549
14. Viswanathan, K., and Früh, K. (2007) Viral proteomics: global evaluation of viruses and their interaction with the host. *Expert Rev. Proteomics* **4,** 815–829
15. Santamaria, E., Mora, M. I., Carro-Roldan, E., Molina, M., Fernández-Irigoyen, J., Marconi, P., Manservigi, R., Greco, A., Epstein, A. L., Prieto, J., Hernández-Alcoceba, R., and Corrales, F. J. (2009) Identification of replication-competent HSV-1 Cgal+ strain targets in a mouse model of human hepatocarcinoma xenograft. *J. Proteomics* **73,** 153–160
16. Santamaria, E., Mora, M. I., Potel, C., Fernández-Irigoyen, J., Carro-Roldán, E., Hernandez-Alcoceba, R., Prieto, J., Epstein, A. L., and Corrales, F. J. (2009) Identification of replication-competent HSV-1 Cgal+ strain signaling targets in human hepatoma cells by functional organelle proteomics. *Mol. Cell. Proteomics* **8,** 805–815
17. Fontaine-Rodriguez, E. C., Taylor, T. J., Olesky, M., and Knipe, D. M. (2004) Proteomics of herpes simplex virus infected cell protein 27: association with translation initiation factors. *Virology* **330,** 487–492
18. Taylor, T. J., and Knipe, D. M. (2004) Proteomics of herpes simplex virus replication compartments: association of cellular DNA replication, repair, recombination, and chromatin remodeling proteins with ICP8. *J. Virol.* **78,** 5856–5866
19. El-Serag, H. B., and Rudolph, K. L. (2007) Hepatocellular carcinoma: epidemiology and molecular carcinogenesis. *Gastroenterology* **132,** 2557–2576
20. Parkin, D. M., Bray, F., Ferlay, J., and Pisani, P. (2005) Global cancer statistics, 2002. *CA Cancer J. Clin.* **55,** 74–108
21. Mullen, J. T., and Tanabe, K. K. (2003) Viral oncolysis for malignant liver tumors. *Ann Surg. Oncol.* **10,** 596–605
22. Blaho, J. A. Oncoapoptosis: a novel molecular therapeutic for cancer treatment. *IUBMB Life* **62,** 87–91
23. Nguyen, M. L., and Blaho, J. A. (2007) Apoptosis during herpes simplex virus infection. *Adv. Virus Res.* **69,** 67–97
24. Shen, Y., and Nemunaitis, J. (2006) Herpes simplex virus 1 (HSV-1) for cancer treatment. *Cancer Gene Ther.* **13,** 975–992
25. Aubert, M., and Blaho, J. A. (2003) Viral oncoapoptosis of human tumor cells. *Gene Ther* **10,** 1437–1445
26. Nguyen, M. L., Kraft, R. M., and Blaho, J. A. (2007) Susceptibility of cancer cells to herpes simplex virus-dependent apoptosis. *J. Gen. Virol.* **88,** 1866–1875
27. Diaz, J. J., Simonin, D., Masse, T., Deviller, P., Kindbeiter, K., Denoroy, L., and Madjar, J. J. (1993). The herpes simplex virus type 1 US11 gene product is a phosphorylated protein found to be non-specifically associated with both ribosomal subunits. *J. Gen. Virol.* **74**, 397–406
28. Sinclair, M. C., McLauchlan, J., Marsden, H., and Brown, S. M. (1994). Characterization of a herpes simplex virus type 1 deletion variant (1703) which under-produces Vmw63 during immediate early conditions of infection. *J. Gen. Virol.* **75**, 1083–1089
29. Johnson, P. A., Best, M. G., Friedmann, T., and Parris, D. S. (1991) Isolation of a herpes simplex virus type 1 mutant deleted for the essential UL42 gene and characterization of its null phenotype. *J. Virol.* **65,** 700–710
30. Santamaria, E., Avila, M. A., Latasa, M. U., Rubio, A., Martin-Duce, A., Lu, S. C., Mato, J. M., and Corrales, F. J. (2003) Functional proteomics of nonalcoholic steatohepatitis: mitochondrial proteins as targets of S-adenosylmethionine. *Proc. Natl. Acad. Sci. U.S.A.* **100,** 3065–3070
31. Dayon, L., Hainard, A., Licker, V., Turck, N., Kuhn, K., Hochstrasser, D. F., Burkhard, P. R., and Sanchez, J. C. (2008) Relative quantification of proteins in human cerebrospinal fluids by MS/MS using 6-plex isobaric tags. *Anal. Chem.* **80,** 2921–2931
32. Smyth, G. K. (2004). Linear models and empirical bayes methods for assessing differential expression in microarray experiments. *Stat. Appl. Genet. Mol. Biol.* **3,** Article3
33. Gentleman, V., Carey, V., Dudoit, S., Irizarry, R., and Huber, W. (2005). *Bioinformatics and computational biology solutions using R and Bioconductor.* Statistics for Biology and Health (Wong, W., Gail, M., Krickeberg, K., Tsiatis, A., and Samet, J., Eds.), Springer, New York
34. Mou, F., Forest, T., and Baines, J. D. (2007) US3 of herpes simplex virus type 1 encodes a promiscuous protein kinase that phosphorylates and alters localization of lamin A/C in infected cells. *J. Virol.* **81,** 6459–6470
35. Galarneau, A., and Richard, S. (2005) Target RNA motif and target mRNAs of the Quaking STAR protein. *Nat. Struct. Mol. Biol.* **12,** 691–698
36. Wu, J., Zhou, L., Tonissen, K., Tee, R., and Artzt, K. (1999) The quaking I-5 protein (QKI-5) has a novel nuclear localization signal and shuttles between the nucleus and the cytoplasm. *J. Biol. Chem.* **274,** 29202–29210
37. Larocque, D., Galarneau, A., Liu, H. N., Scott, M., Almazan, G., and Richard, S. (2005) Protection of p27(Kip1) mRNA by quaking RNA binding proteins promotes oligodendrocyte differentiation. *Nat. Neurosci.* **8,** 27–33
38. Yang, G., Fu, H., Zhang, J., Lu, X., Yu, F., Jin, L., Bai, L., Huang, B., Shen, L., Feng, Y., Yao, L., and Lu, Z. RNA-binding protein quaking, a critical regulator of colon epithelial differentiation and a suppressor of colon cancer. *Gastroenterology* **138,** 231–240, e231–235
39. Susaki, E., Nakayama, K., Yamasaki, L., and Nakayama, K. I. (2009) Common and specific roles of the related CDK inhibitors p27 and p57 revealed by a knock-in mouse model. *Proc. Natl. Acad. Sci. U.S.A.* **106,** 5192–5197
40. Hardy, R. J. (1998) QKI expression is regulated during neuron-glial cell fate decisions. *J. Neurosci. Res.* **54,** 46–57
41. Krummenacher, C., Baribaud, I., Eisenberg, R. J., and Cohen, G. H. (2003) Cellular localization of nectin-1 and glycoprotein D during herpes simplex virus infection. *J. Virol.* **77,** 8985–8999
42. Foka, P., Pourchet, A., Hernandez-Alcoceba, R., Doumba, P. P., Pissas, G., Kouvatsis, V., Dalagiorgou, G., Kazazi, D., Marconi, P., Foschini, M., Manservigi, R., Konstadoulakis, M. M., Koskinas, J., Epstein, A. L., and Mavromara, P. (2010). Novel tumour-specific promoters for transcriptional targeting of hepatocellular carcinoma by herpes simplex virus vectors. *J. Gene Med.*
43. Tannu, N. S., and Hemby, S. E. (2006) Two-dimensional fluorescence difference gel electrophoresis for comparative proteomics profiling. *Nat. Protoc.* **1,** 1732–1742
44. Liu, P., O'Mara, B. W., Warrack, B. M., Wu, W., Huang, Y., Zhang, Y., Zhao, R., Lin, M., Ackerman, M. S., Hocknell, P. K., Chen, G., Tao, L., Rieble, S., Wang, J., Wang-Iverson, D. B., Tymiak, A. A., Grace, M. J., and Russell, R. J. (2010) A tris (2-carboxyethyl) phosphine (TCEP) related cleavage on cysteine-containing proteins. *J. Am. Soc. Mass Spectrom.* **21,** 837–844
45. Wang, Z., Rejtar, T., Zhou, Z. S., and Karger, B. L. (2010) Desulfurization of cysteine-containing peptides resulting from sample preparation for protein characterization by mass spectrometry. *Rapid Commun. Mass Spectrom.* **24,** 267–275
46. Tiberti, N., Hainard, A., Lejon, V., Robin, X., Mumba Ngoyi, D., Turck, N., Matovu, E., Enyaru, J., Mathu Ndung, U. J., Scherl, A., Dayon, L., and Sanchez, J. C. (2010). Discovery and verification of osteopontin and beta-2-microglobulin as promising markers for staging human African trypanosomiasis. *Mol. Cell Proteomics.*
47. Larocque, D., and Richard, S. (2005) QUAKING KH domain proteins as regulators of glial cell fate and myelination. *RNA Biol.* **2,** 37–40
48. Chénard, C. A., and Richard, S. (2008) New implications for the QUAKING RNA binding protein in human disease. *J. Neurosci. Res.* **86,** 233–242
49. Li, Z., Takakura, N., Oike, Y., Imanaka, T., Araki, K., Suda, T., Kaname, T., Kondo, T., Abe, K., and Yamamura, K. (2003) Defective smooth muscle development in qkI-deficient mice. *Dev. Growth Differ.* **45,** 449–462
50. Larocque, D., Fragoso, G., Huang, J., Mushynski, W. E., Loignon, M., Richard, S., and Almazan, G. (2009) The QKI-6 and QKI-7 RNA binding proteins block proliferation and promote Schwann cell myelination. *PLoS One* **4,** e5867
51. Vlachos, P., Nyman, U., Hajji, N., and Joseph, B. (2007) The cell cycle

inhibitor p57(Kip2) promotes cell death via the mitochondrial apoptotic pathway. *Cell Death Differ.* **14,** 1497–1507
52. Zhu, Z., Cai, W., and Schaffer, P. A. (1994) Cooperativity among herpes simplex virus type 1 immediate-early regulatory proteins: ICP4 and ICP27 affect the intracellular localization of ICP0. *J. Virol.* **68,** 3027–3040
53. Sedlackova, L., and Rice, S. A. (2008) Herpes simplex virus type 1 immediate-early protein ICP27 is required for efficient incorporation of ICP0 and ICP4 into virions. *J. Virol.* **82,** 268–277
54. Cai, W., and Schaffer, P. A. (1992) Herpes simplex virus type 1 ICP0 regulates expression of immediate-early, early, and late genes in productively infected cells. *J. Virol.* **66,** 2904–2915
55. Chen, J., and Silverstein, S. (1992) Herpes simplex viruses with mutations in the gene encoding ICP0 are defective in gene expression. *J. Virol.* **66,** 2916–2927
56. Gelman, I. H., and Silverstein, S. (1985) Identification of immediate early genes from herpes simplex virus that transactivate the virus thymidine kinase gene. *Proc. Natl. Acad. Sci. U.S.A.* **82,** 5265–5269
57. Quinlan, M. P., and Knipe, D. M. (1985) Stimulation of expression of a herpes simplex virus DNA-binding protein by two viral functions. *Mol. Cell. Biol.* **5,** 957–963
58. DeLuca, N. A., and Schaffer, P. A. (1985) Activation of immediate-early, early, and late promoters by temperature-sensitive and wild-type forms of herpes simplex virus type 1 protein ICP4. *Mol. Cell. Biol.* **5,** 1997–2008
59. Sampath, P., and Deluca, N. A. (2008) Binding of ICP4, TATA-binding protein, and RNA polymerase II to herpes simplex virus type 1 immediate-early, early, and late promoters in virus-infected cells. *J. Virol.* **82,** 2339–2349
60. Zabierowski, S., and DeLuca, N. A. (2004) Differential cellular requirements for activation of herpes simplex virus type 1 early (tk) and late (gC) promoters by ICP4. *J. Virol.* **78,** 6162–6170
61. McGregor, F., Phelan, A., Dunlop, J., and Clements, J. B. (1996) Regulation of herpes simplex virus poly (A) site usage and the action of immediate-early protein IE63 in the early-late switch. *J. Virol.* **70,** 1931–1940
62. Uprichard, S. L., and Knipe, D. M. (1996) Herpes simplex ICP27 mutant viruses exhibit reduced expression of specific DNA replication genes. *J. Virol.* **70,** 1969–1980
63. Jean, S., LeVan, K. M., Song, B., Levine, M., and Knipe, D. M. (2001) Herpes simplex virus 1 ICP27 is required for transcription of two viral late (gamma 2) genes in infected cells. *Virology* **283,** 273–284
64. Reddy, T. R., Suhasini, M., Xu, W., Yeh, L. Y., Yang, J. P., Wu, J., Artzt, K., and Wong-Staal, F. (2002) A role for KH domain proteins (Sam68-like mammalian proteins and quaking proteins) in the post-transcriptional regulation of HIV replication. *J. Biol. Chem.* **277,** 5778–5784
65. Everett, R. D., Sourvinos, G., Leiper, C., Clements, J. B., and Orr, A. (2004) Formation of nuclear foci of the herpes simplex virus type 1 regulatory protein ICP4 at early times of infection: localization, dynamics, recruitment of ICP27, and evidence for the de novo induction of ND10-like complexes. *J. Virol.* **78,** 1903–1917
66. Livingston, C. M., Ifrim, M. F., Cowan, A. E., and Weller, S. K. (2009). Virus-Induced Chaperone-Enriched (VICE) domains function as nuclear protein quality control centers during HSV-1 infection. *PLoS Pathog.* **5,** e1000619
67. Zhang, Y., Lu, Z., Ku, L., Chen, Y., Wang, H., and Feng, Y. (2003) Tyrosine phosphorylation of QKI mediates developmental signals to regulate mRNA metabolism. *EMBO J.* **22,** 1801–1810
68. Côte, J., Boisvert, F. M., Boulanger, M. C., Bedford, M. T., and Richard, S. (2003) Sam68 RNA binding protein is an in vivo substrate for protein arginine N-methyltransferase 1. *Mol. Biol. Cell* **14,** 274–287
69. Piñol-Roma, S., and Dreyfuss, G. (1991) Transcription-dependent and transcription-independent nuclear transport of hnRNP proteins. *Science* **253,** 312–314
70. Piñol-Roma, S., and Dreyfuss, G. (1992) Shuttling of pre-mRNA binding proteins between nucleus and cytoplasm. *Nature* **355,** 730–732
71. Bastian, T. W., and Rice, S. A. (2009) Identification of sequences in herpes simplex virus type 1 ICP22 that influence RNA polymerase II modification and viral late gene expression. *J. Virol.* **83,** 128–139
72. Marozin, S., Prank, U., and Sodeik, B. (2004) Herpes simplex virus type 1 infection of polarized epithelial cells requires microtubules and access to receptors present at cell-cell contact sites. *J. Gen Virol.* **85,** 775–786
73. Krummenacher, C., Baribaud, I., Sanzo, J. F., Cohen, G. H., and Eisenberg, R. J. (2002) Effects of herpes simplex virus on structure and function of nectin-1/HveC. *J. Virol.* **76,** 2424–2433
74. Geraghty, R. J., Krummenacher, C., Cohen, G. H., Eisenberg, R. J., and Spear, P. G. (1998) Entry of alphaherpesviruses mediated by poliovirus receptor-related protein 1 and poliovirus receptor. *Science* **280,** 1618–1620
75. Sakisaka, T., Taniguchi, T., Nakanishi, H., Takahashi, K., Miyahara, M., Ikeda, W., Yokoyama, S., Peng, Y. F., Yamanishi, K., and Takai, Y. (2001) Requirement of interaction of nectin-1alpha/HveC with afadin for efficient cell-cell spread of herpes simplex virus type 1. *J. Virol.* **75,** 4734–4743
76. Even, D. L., Henley, A. M., and Geraghty, R. J. (2006) The requirements for herpes simplex virus type 1 cell-cell spread via nectin-1 parallel those for virus entry. *Virus Res.* **119,** 195–207